

Evaluating Current Distribution and Influence of Defect Sites for Graphitic Compound Bipolar Plate Materials

Journal Article**Author(s):**

Baumann, Nils; Blankenship, Andrea; Dorn, Marvin; Cremers, Carsten

Publication date:

2020-02

Permanent link:

<https://doi.org/10.3929/ethz-b-000387184>

Rights / license:

[Creative Commons Attribution 4.0 International](#)

Originally published in:

Fuel Cells 20(1), <https://doi.org/10.1002/fuce.201900138>



Evaluating Current Distribution and Influence of Defect Sites for Graphitic Compound Bipolar Plate Materials

N. Baumann^{1*}, A. Blankenship^{1,2}, M. Dorn¹, C. Cremers¹

¹ Fraunhofer-Institut für Chemische Technologie ICT, Angewandte Elektrochemie, Joseph-von-Fraunhofer-Straße 7, 76327 Pfinztal, Germany

² Present address: ETH Zürich, Department of Chemistry and Applied Biosciences, Vladimir-Prelog Weg 1-5/10, 8093 Zürich, Switzerland

Received July 29, 2019; accepted November 23, 2019; published online December 18, 2019

Abstract

With the growth in power and size of energy conversion devices, the consideration of current distribution inside cells and stacks becomes increasingly important. In light of understanding the effect of the material properties of graphitic compound materials on current distribution, we developed a novel measurement cell based on a segmented current feed and a segmented measurement board. Using this cell, we determined the cross-conduction of current in three commercial graphitic compound materials used for the manufacturing of bipolar plates. The conduction behaviors, with respect to compacting pressure as well as total current density, were

explained by differences in resistance of conduction pathways. Large observed differences between the materials were discussed in terms of the ratio of through-plane and in-plane resistivities. Additionally, we compared several methods to emulate defect sites, in order to evaluate their effect using the novel measurement cell and showed the effect of their size on the current distribution. Finally, we discuss improvements on the measurement setup.


Keywords: Bipolar Plate, Conducting Materials, Current Distribution Measurement, Defect Sites, Energy Conversion, Fuel Cell, In-plane Resistivity, Measurement Technique, Through-plane Resistivity

1 Introduction

Considering the environmental, economic and political driving forces to reduce CO₂ emissions and to increase the use of renewable electricity, energy conversion and storage devices are increasingly important. Bipolar plates (BPP) are a key component in devices such as fuel cells or electrolyzers. BPPs separate each cell in a stack, and thereby provide a barrier for gas crossover and structural stability. Additionally, they guarantee the electronic connection between each cell and, therefore, must have a high electronic conductivity. Consequently, BPPs play a major role in terms of cost [1], performance, and long term stability of such energy conversion systems [2]. As devices increase in power, so usually do the size of the electrodes and correspondingly the size of the BPPs. Using larger electrodes can be an issue due to the homogeneity of the reactions, e.g., from catalyst blocking due to the collection of water droplets in proton exchange membrane (PEM) fuel cells or areas of decreased contact resistance resulting from protruding gas diffusion layer fibers, leading to inhomogeneous current distribution over the electrode and BPP [3]. In

the worst case, these issues/defects can lead to hot-spots of high current density and high temperature, potentially damaging the membrane through material degradation and the formation of pinholes, thereby decreasing the cell and system lifetime [4]. Cells, and more specifically BBPs, therefore need to be able to tolerate current density inhomogeneity and distribute the current in-plane to mitigate degradation. Another aspect of local defect sites in combination with low in-plane conductivity is the problem of proliferation of sites with low or no activity in a single electrode throughout the whole stack, drastically reducing performance even in cells that would otherwise show unimpaired activity, as illustrated in Figure 1 [5]. In Figure 1, arrows in the schematic represent current flow. For clarity purposes, in-plane current flow is only shown at

[*] Corresponding author, nils.baumann@ict.fraunhofer.de

 This is an open access article under the terms of the Creative Commons Attribution License, which permits use, distribution and reproduction in any medium, provided the original work is properly cited.

the defect site. The red area in the center drawing represents an area of reduced current flow originating at the defect site and propagating through the stack. Thus, the ratio of in-plane to through-plane conductivity of the BPP is a relevant characteristic that influences current density distribution in the cell and the stack. Plain/uncoated metallic materials for BPPs are not expected to present this issue, as metals show isotropic conductivity throughout the sample. This maybe different on the structured BPP level, where the current transfer from one half-plate to the next should also be locally different, due to different distances between contact points. Entire structured BPPs were, however, not investigated within this study. Due to the possible corrosion of metallic (especially steel) BPPs [6–9] and the corresponding need to coat them [10–12], graphitic compound materials are employed in many cases, in particular when long lifetimes are required, e.g., in high temperature (HT) PEM-FCs. These graphite compound BPPs are typically made from a polymer matrix, e.g., polypropylene (PP), polyphenylene sulfide (PPS) or polyvinylidene fluoride (PVDF), to which a highly conductive graphitic filler material is added [2]. Manufacturing parameters as well as the type, amount, and orientation of filler material can influence the electronic properties of these compound materials. Caglar et al. [13], for instance, have shown that the in-plane conductivity of a graphite/PPS compound can be improved by adding carbon nanotubes (CNTs). The authors assign this effect to CNTs serving as bridges between graphite particles, a mechanism that should be transferable to other graphite/polymer compounds.

Even though there are many studies on the measurement of through-plane and in-plane conductivity [14–19], they are only studies determining these values as a global parameter. To the best of our knowledge, there are no reports on experimental evaluation of in-plane current distribution in graphitic materials. Although there is research on cell characteristics (current density and temperature) using segmented cell technology [20–24], none of the studies, to our knowledge, specifically look at the influence of the conductivities of the BPP material. Instead, these studies use membrane electrode assemblies (MEAs) and investigate conditions causing inhomogeneous current generation but do not measure its propagation or compensation. Additionally, there are other studies using the segmented cell technology to evaluate the influence of different fuel concentrations [25]. These studies, however, do not represent a systematic analysis of the influence of defect size on current density homogeneity. Only Phillips et al. [26] looked at defect sizes in the sense that they fabricated a membrane electrode assembly with different masks covering the membrane, such that part of the membrane was not coated with the catalyst layer. In contrast to our work, the authors only studied four different sizes and, again, the additional cell components in their study add more complexity.

In this study, we report on the setup of a new measurement cell to evaluate in-plane current distribution of graphitic BPP

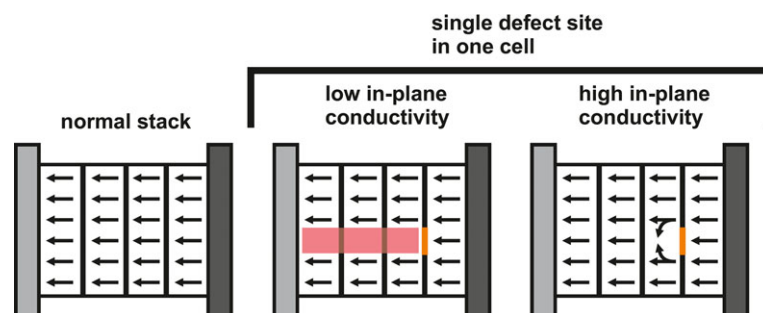


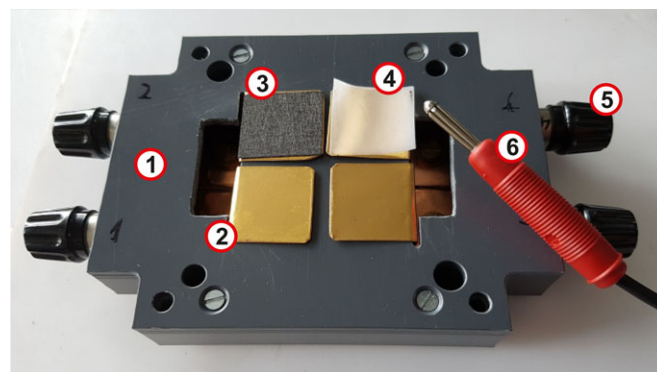
Fig. 1 Current flow in normal stack (left), in a stack with a single defect site and bipolar plates with low in-plane conductivity (relative to through-plane conductivity, center) and in a stack with a single defect site and bipolar plates with high in-plane conductivity (relative to through-plane conductivity, right).

materials, as used in applications for PEM fuel cells, based on a segmented current feed and measurement of local exit-current distribution. Furthermore, we determined the influence of different sizes of defect sites consisting of materials that either increase or decrease contact resistance on the cell and, as a result, affect the local current distribution within the cell.

2 Experimental

2.1 Construction of Measurement Cell

Our in-house developed measurement cell is based on the cell holder of the quickConnect fixture qCf FC25/100 (balticFuelCells GmbH, Germany) and consists of a customized housing, analogous to the balticFuelCells cell holder. One component holds the sample itself, which is a 3 mm thick graphitic BPP in this study. The sample is connected to the 7×7 segments current scan line segmented measurement cell (S++ Simulation Services, Germany). The other side of the cell holder (shown in Figure 2) includes four copper segments, which act as current feeds and are gold-coated to decrease contact resistance. Gas diffusion layers (GDL) are placed between the copper electrode and the sample to improve electrical contact between the two rigid surfaces by compensating



1 - Polymer casing
2 - Gold coated copper sheet
3 - Gas diffusion layer
4 - PTFE sheet
5 - Cable connection
6 - Contact cable

Fig. 2 Measurement cell.

for surface irregularities. Each copper segment is connected individually to a banana jack. All cables from selected segments are joined through a metallic rail to a single cable connected to the potentiostat (HCP-803, BioLogic, France). Using this configuration, we are able to generate different locally-controlled current densities across the surface of the sample and measure the in-plane current distribution in the BPPs of different materials.

2.2 Evaluation of Current Distribution

As a means to quantitatively evaluate different materials and measurement parameters, we placed two segments located diagonally from each other on one side of the material, connected both to the working electrode cable of the potentiostat, and applied a fixed current to the working electrode, see also Figure 3A. The percentage of the total current flowing through the area under the non-connected segments is then a value proportional to the ability to distribute the current in-plane and to tolerate current density inhomogeneity. For the calculation of the cross-conducted current, the currents through all segments excluding both 3×3 segments under the copper contact sheets were summed, see blue highlighted segments in Figure 3B. The cell holder is pressed together in the fixture using a pneumatic cylinder (piston), and the influence of the pressure on the cell holder was determined by applying current densities of 1 A cm^{-2} and 2 A cm^{-2} with respect to the area of the connected segments and then varying the pressure on the piston. Further measurements determined the cross-conducted current as a function of total current density for three different commercial graphitic BPP materials (in the fol-

lowing paper referred to as graphite compound A, B and C) applying current densities up to 2 A cm^{-2} .

2.3 Evaluation of Defect Sites

For the evaluation of defect sites, the measurement configuration with two diagonally-located electrically-connected copper segments from before was maintained. An artificial defect site was placed under the center of one copper electrode segment, as shown in Figure 3A, so that it lay facing one of smaller segments of the segmented S++ board on the opposite side of the BPP. The defect site had the shape of a circle with varying sizes from 2–14 mm in diameter. For a comparison of different defect sizes to the measurement segments of the S++, see Figure 3C. In order to evaluate the best method to emulate defect sites, four different configurations were tested, as shown as cross section in Figure 3D: (i) The BPP was spin-coated (Spin150, SPS-Europe B.V., Netherlands) with positive photoresist ma-P 1215 (Micro Resist Technology GmbH, Germany). After curing at 110°C , a template mask with a circular defect site was placed on top of the coated BPP, and the coated plate was subsequently exposed to UV radiation as directed in the photoresist manufacturer's protocol. The photoresist on the BPP exposed to UV radiation was then stripped from the plate using a 0.5 M NaOH solution, leaving behind only the circular section of non-exposed photoresist as the defect site. The thickness of the photoresist layer was determined by coating half of a glass slide with photoresist and using a confocal microscope (μsurf custom, NanoFocus AG, Germany) to measure the height of the edge. (ii) Two different PTFE sheets with $80 \mu\text{m}$ and $160 \mu\text{m}$ thicknesses were placed between the BPP

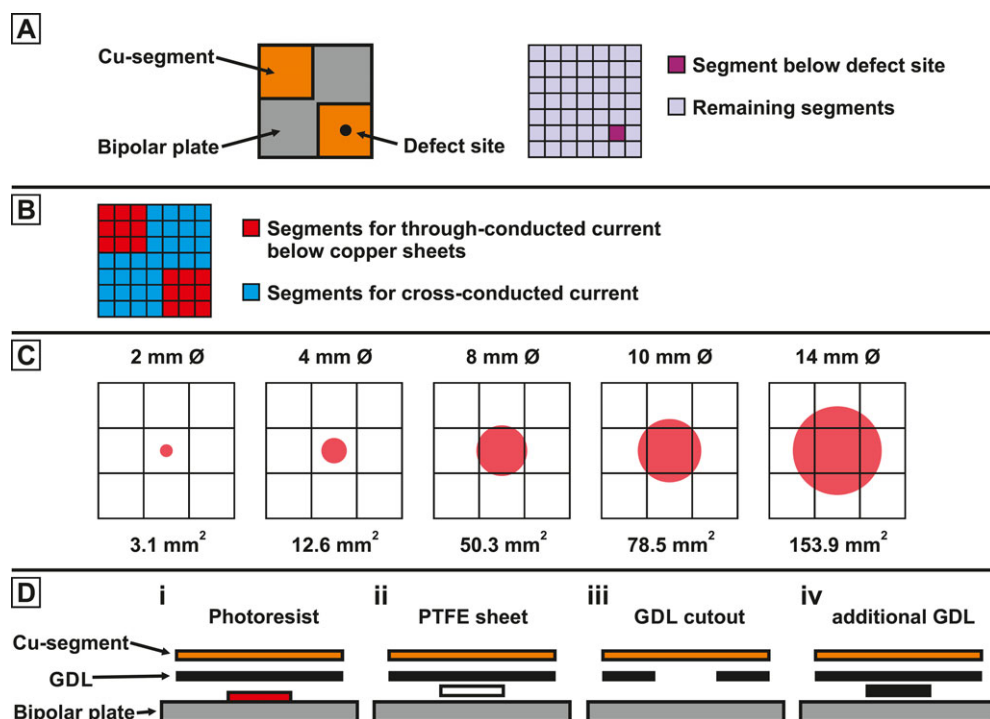


Fig. 3 (A) Connected segments and location of defect site. (B) Different segments for the evaluation of current distribution. (C) Comparison of size of defect site to the size of the measurement segment of the S++. (D) Different methods to simulate defect sites.

sample and the contact GDL. (iii) A hole with the appropriate size was punched out of the contact GDL placed on the BPP. (iv) An additional GDL sheet was placed between the BPP sample and the contact GDL. Method (iv) was the only method that was devised to emulate a defect site with an increased activity, i.e., higher current flowing through this site compared to the surrounding area.

Results of the defect sites were analyzed in terms of the fraction of current passing through the segment directly under the defect site with respect to the current through all segments, as illustrated in Figure 3A.

3 Results and Discussion

3.1 Current Distribution

Measurement of the influence of the piston pressure on the cell holder was investigated for one material (graphite compound A). Figure 4 shows the influence of the pressure for two current densities. Two measurements at each pressure were recorded. Values given in Figure 4 represent the average, whereas the error bar represents the lower and higher measured value. A slight increase in cross-conducted current with increasing compacting pressure can be observed for the lower current density, although the scatter was rather large so that the increase lies within the error bar for this measurement. At higher current densities, the compacting pressure did not have an influence. The observed increase could be explained by a more uniform contact of the GDL to the surface of the sample, especially at the edges of the copper contact sheet. Also, the GDL is compressed to a higher degree, increasing its conductivity [27,28]. For all following measurements, a compacting pressure of 5 bar (1.5 N mm^{-2}) was chosen.

The influence of the total current density on the cross-conducted current can be seen in Figure 5 for all three compound materials. Lines in Figure 5 are only given for visual guidance. It is evident that there are huge differences in the ability to conduct current in-plane depending on the material. Table 1

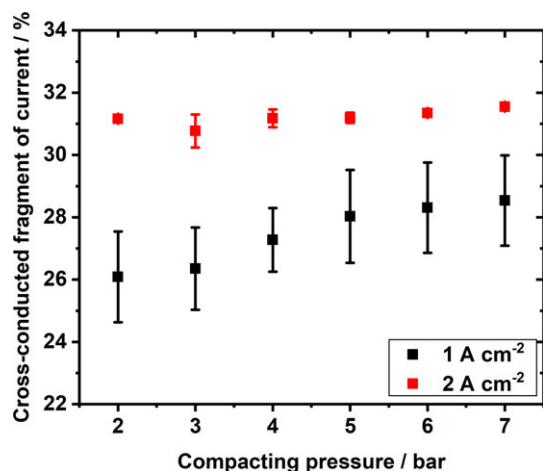


Fig. 4 Cross-conducted fragment of current vs. compacting pressure of the piston.

lists the in-plane and through-plane specific electrical resistivities (as given by the material datasheet of the manufacturer) as well as the ratio of the two. While the through-plane resistivities are fairly similar, the in-plane resistivity of graphite compound B is close to a factor of three higher than the respective values of the other compounds. This can be correlated to the behavior seen in Figure 5, which shows similar curves only for compound A and C and a different curve for compound B.

The much higher in-plane electrical resistivity leads to a lower fraction of the current being cross-conducted inside the sample, though the percentage for compound B is not a factor of three lower than the percentage of the other compounds. However, if the through-plane to in-plane resistivity ratio is compared, compound B only lies a factor of two lower than compounds A and C, matching more closely the observed behavior in Figure 5. Although it was expected that the cross-conduction correlates with in-plane resistivity, it seems it is not the only limiting factor. The nature of the graphitic filler material and especially its distribution inside the sample certainly play a role as well. It is possible that the material properties of the polymer matrix, which are different among the samples, have an influence. Lastly, manufacturing defect sites such as fractures or air pockets inside of the material will have an impact on current distribution as well, although visible inspection and scanning electron microscopy (SEM) images of cross sections did not reveal any such details. A cross section

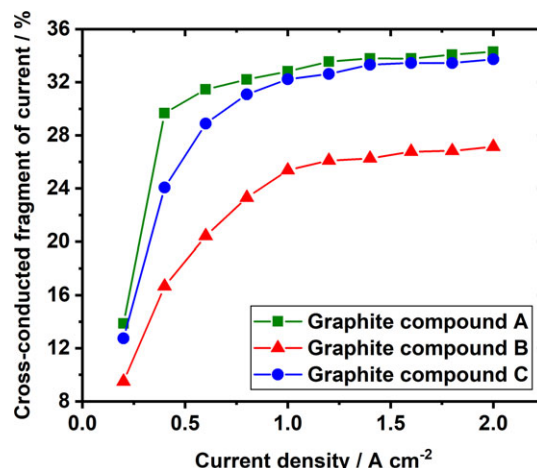


Fig. 5 Cross-conducted fragment of current vs. total current density.

Table 1 Specific electrical resistivities of the used graphite compounds.

Material	Specific electrical resistivity through-plane / $\Omega \text{ cm}$	Specific electrical resistivity in-plane / $\Omega \text{ cm}$	Ratio of through-plane to in-plane resistivity
Graphite compound A	0.28	0.014	20.0
Graphite compound B	0.31	0.034	9.12
Graphite compound C	0.24	0.010	24.0

only images a specific slice of the material, and therefore it is possible some defects within the BPP were not captured.

A steeply rising fragment of cross-conducted current with increasing current density (for low current densities) is apparent for all three samples. With higher current densities, the cross-conduction levels off quickly for all samples as well, but the level at which this happens varies with the material. While the value starts to level off around 0.5 A cm^{-2} for graphite compound A and at around 0.75 A cm^{-2} for graphite compound C, for graphite compound B it continues to rise to about 1 A cm^{-2} . The observation of improving conduction of current within the plane of the material with increasing current density could be explained by the conduction mechanism in polymeric compound materials based on a non-conducting matrix and a highly conductive filler material. Since the filler particles are randomly distributed in the material, individual conduction pathways can have a different overall resistance depending on number of touching particles, contact area between touching particles, and overall length of the conduction pathway. Moreover, as described for instance by Li et al. [29] for a CNT-filled compound, another important factor in the conduction mechanism is the tunneling resistance between neighboring filler particles, in the case of their study, CNTs. When the current is increased, the voltage drop across the cell is increased as well. With increasing voltage, more conduction pathways become active as their conduction resistance is overcome, contributing to a higher percentage of cross-conducted current. This also levels off, as at a certain voltage no more pathways are inactive. Since most commercial energy conversion systems are operated at current densities above 1 A cm^{-2} the cross-conductivity of the graphite compound material will have reached its maximum extent. This explanation is also in agreement with the results of Figure 4, where a lower dependence of the cross-conducted current on compacting pressure was observed with higher current densities.

3.2 Size of Defect Sites

In order to evaluate the influence of the size of the defect site, graphite compound A was used as the sample material. The fragment of current through the segment below the defect site with respect to the current through the remaining segments as a function of area of defect site is shown in Figure 6 for all methods. All data points are an average of four measurements, and error bars represent the standard deviation. The blue points represent the reference measurement with no defect site. Considering that 18 segments of the segmented measurement board were below the copper electrodes, one would expect a fraction of 0.055 in one such segment, which is seen in Figure 6. However, as was shown earlier, at 1 A cm^{-2} roughly 32% of the total current flows through the other segments. Leaving 68% of the total current through the segments below the copper electrodes should give a value of 0.037 for a single segment. This discrepancy is most likely due to the inhomogeneity of the current distribution. As can be seen in Figure 7, the current at the segments below the two copper

electrodes varies not just depending on the electrode, but also depending on the exact segment. Since the electrical conductivity of the sample and all involved components (copper sheet, GDL) is very high, even small differences, in for example contact resistance, will result in different currents flowing through the particular parts of the sample. This variation can also explain why some measurement points in Figure 6 deviate from the observed trend of the respective measurement series. As the lower right copper electrode showed a more uniform current distribution, the defect site was placed in the center of that electrode.

Coating the sample with photoresist offers the best control in terms of exact location and size/shape of the defect site. Although the value at 3 mm diameter (7.01 mm^2 area) is significantly lower than at 2 mm diameter (3.14 mm^2 area), the values actually increase again with 4 mm diameter (12.6 mm^2 area) and 5 mm diameter (19.6 mm^2 area). Thus, no clear trend can be observed. Considering the thickness of the resist layer

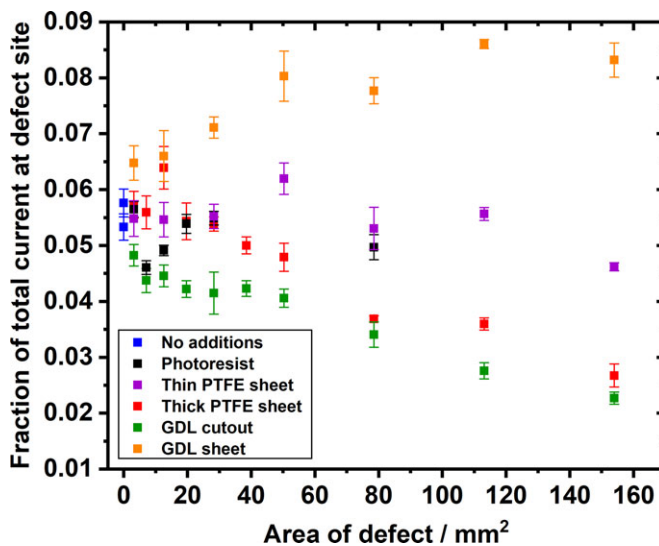


Fig. 6 Fraction of current under defect site as a function of defect site area for different methods.

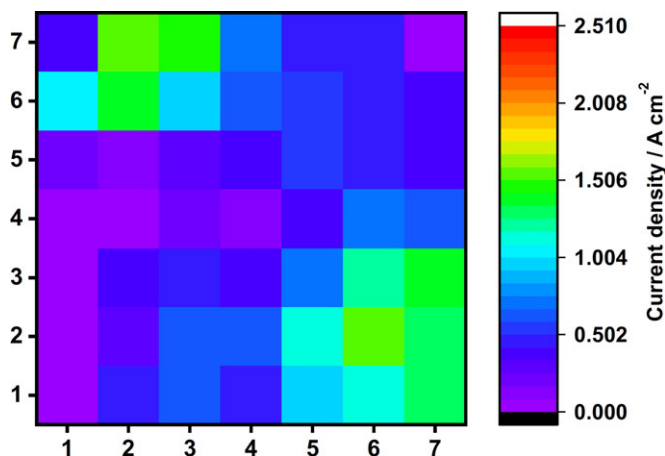


Fig. 7 Current density map of graphite compound A at 1 A cm^{-2} total current with no defect site.

is only 20 μm , as measured by confocal microscopy, the reduction in conductivity is apparently not sufficient to adequately emulate a defect site with no activity in a fuel cell or electrolyzer.

The same is true for the thin (80 μm thickness) PTFE sheet, which has roughly the same values for all sizes, with the one at 8 mm diameter (50.3 mm^2 area) showing a significantly larger fraction of current at the defect size and the one at 14 mm diameter (153.9 mm^2 area) a significantly lower fraction. Although a good trend can be seen for the thicker PTFE sheet, the values seem to be still quite large, given the fact that PTFE has a very low electrical conductivity of around $5 \times 10^{-17} \text{ S m}^{-1}$ [30]. Part of this can be explained by the fact that some current flows back into the area of the defect from around it due to the cross-conductivity of the graphitic BPP material, which is exactly what the BPP is supposed to achieve. Another aspect to consider is the compression of the GDL. The PTFE sheet thicknesses are roughly half and the same as the GDL for the thin and thick sheets, respectively. This means that the GDL gets compressed considerably at the defect site. As Kleeemann et al. [27] have reported, the electrical conductivity of woven carbon fiber GDL increases considerably with increasing compression, especially at low compression pressures. Nitta et al. [28] also evaluated conductivity behavior of GDL at different compressions and found increasing conductivity at higher compression, which the authors attribute to a decrease in porosity and, consequently, an increase in fiber contact area. In our case, this means that the decrease in conductivity through the PTFE sheet is partly compensated by the increase in conductivity through the compressed GDL. To validate this explanation, a second GDL sheet was inserted into the cell in place of the PTFE sheet. As can be seen in Figure 6, the current at the defect site increases with the defect area, showing that the increased conductivity due to GDL compression can account for the observed results. It also shows that, by using this method, both low and high activity defects can be emulated and evaluated for graphitic compound materials.

The lowest currents at the defect site were achieved by using GDLs with punched-out holes as defect sites. Since no additional layer is introduced into the system, no GDL compression occurs, and thus the low currents can be explained. Example current density maps can be seen in Figure 8, with the segment below the defect site being marked with an arrow in Figure 8A. On the left side, both a slight increase in current density at the defect site for the PTFE

sheet (A) and a large increase for the additional GDL sheet (C) can be seen clearly. It is interesting to observe that the PTFE sheet defect site leads to a decrease in current density in a much larger area, as seen in Figure 8B, whereas the GDL cutout has a well-defined defect site, Figure 8D. As the overall current density was kept constant, the second copper electrode shows a much larger current density in case of the thick PTFE sheet, 14 mm diameter. A reason for the different behavior could lie in the fact that the thick PTFE sheet prevents a clearly defined defect site, as the GDL is bent a little at the edges of the PTFE sheet, preventing good contact with the sample over an area larger than the actual PTFE sheet.

Using thick PTFE sheets and a GDL cutout, the reduction in current at the defect site is nearly linear with respect to increasing defect area, as shown in Figure 9. The larger variation of values for the PTFE sheet can be explained by the higher uncertainty in placing the sheet between the GDL and the sample and possible small shifts of the layer during assembly, whereas the placement of the large GDL with the hole in it was easier to maintain reproducibly. These measurements show that a significant reduction in current density at the defect site is only observed at very large defect sizes, which cannot occur inside fuel cells or electrolyzers from small water droplets or gas bubbles, respectively. Their sizes are restricted by the channel width of the flow fields that are machined into the BPP, and are typically 0.5–2 mm in width [31, 32]. Depending on the exact flow field pattern, this means that a defect extension in one dimension of several millimeters and even centimeters could occur. Even at the largest defect sites, the reduction in current density is only roughly a factor of two,

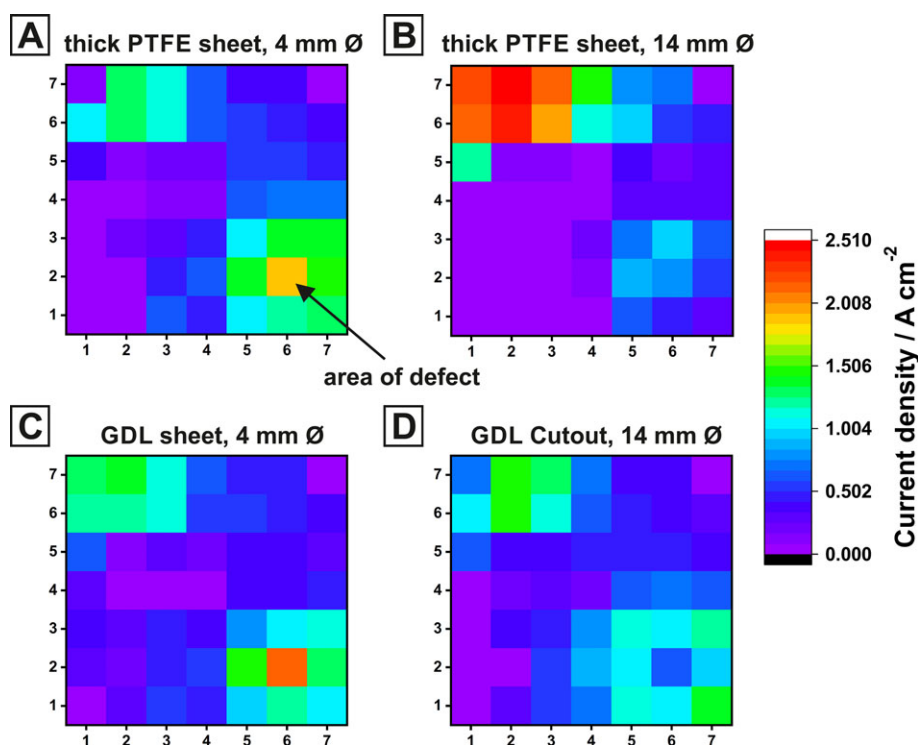


Fig. 8 Current density maps of different defect site measurements.

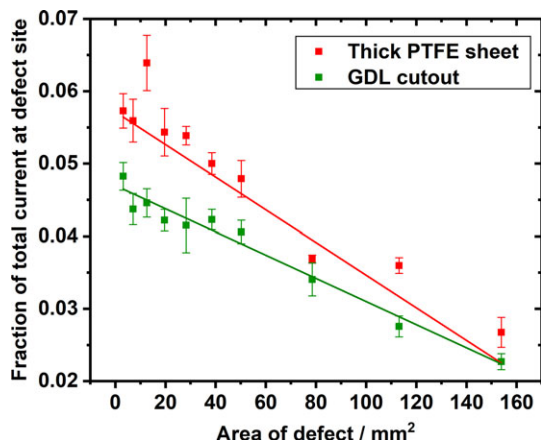


Fig. 9 Fraction of current under defect site as a function of defect site area for thick PTFE sheet and GDL cutout and respective linear regressions.

which means that even for no activity at the defect site, the investigated graphitic material is able to provide reasonable cross-conductivity. However, the investigated material (graphite compound A) was the one with the highest in-plane conductivity, and future experiments will have to show how materials with lower conductivity behave.

3.3 Improvement of Measurement Setup

In light of the promising results and the encountered issues, we devised several improvements on the measurement setup. In order to gain a higher local resolution of the current feed, we changed the cell contact electrodes from four large gold-coated copper sheets to an array of 7×7 spring-contact pins. These pins are commercially available electronic parts and are fixed in a specially designed cell top. Aside from gaining a higher resolution for controlling the current feed into the sample, changing the electrodes is supposed to resolve several other issues. For instance, the contact homogeneity of the large copper electrodes to the sample was achieved by using additional GDL. By using small spring-contact pins, this additional GDL layer can be omitted, as the smaller contact area means that surface irregularities are less of an issue. Larger variations in thickness over the sample can also be compensated for, as the position of each pin is individually controlled by its spring.

In the new cell design, each pin is individually electrically connected, so the emulation of a defect site can be achieved by disconnecting the desired pin or pins. Thus, a much simpler experimental design is possible, in which the position and size (by disconnecting several pins) of the defect site can be controlled and varied quickly and without effort. Moreover, no perturbations of additional layers (e.g., PTFE sheets) are introduced into the setup, which do have a considerable influence, as shown in this paper. It is also conceivable, by including suitable electronic components, to have individual pins not disconnected entirely, but to control their input current precisely. We are currently in the process of setting up this new

measurement cell and will report on its use to measure the effect of defect sites on current distribution inside graphitic compound BPP material in a future paper.

4 Conclusions

We have shown the design and construction of a measurement cell to investigate the current distribution inside graphitic compound materials. The cell is based on a segmented current feed using an array of electrodes on one side of the sample and a segmented measurement board on the other side. Thus, an inhomogeneous current distribution can be induced and the sample's ability to cross-conduct the current in-plane can be evaluated. Large differences in this ability were observed for three different commercial graphitic compound materials, although the general trend of steeply increasing cross-conduction and a following leveling-off with increasing total current density was observed for all samples and explained by different resistances of conduction pathways inside the material.

Furthermore, several methods to induce defect sites in the current distribution measurement were evaluated. It was found that the methods of using a PTFE sheet and punching out a hole in the contact GDL were best suited to achieve a defect site with reduced current. A linearly decreasing current at the defect site with respect to the defect site area was found for these two methods. Lastly, several improvements on the measurement cell were presented in the form of an array of individually connected spring-contact pins in place of the large copper sheet electrodes and GDL contact sheet.

Acknowledgements

Financial support by German Federal Ministry of Transport and Digital Infrastructure (BMVI) under coordination by NOW GmbH for the project BePPel, contract number 03B11002E/03B11002E2, is greatly acknowledged.

References

- [1] A. De las Heras, F. J. Vivas, F. Segura, J. M. Andújar, *Renewable and Sustainable Energy Reviews* **2018**, *96*, 29.
- [2] R. A. Antunes, M. C. L. de Oliveira, G. Ett, V. Ett, *Journal of Power Sources* **2011**, *196*, 2945.
- [3] J. Wang, *Energy* **2015**, *80*, 509.
- [4] A. M. Dafalla, F. Jiang, *International Journal of Hydrogen Energy* **2018**, *43*, 2327.
- [5] M. Müller, J. Hirschfeld, R. Lambertz, A. Schulze Lohoff, H. Lustfeld, H. Pfeifer, M. Reißel, *Journal of Power Sources* **2014**, *272*, 225.
- [6] S. Lædre, O. E. Kongstein, A. Oedegaard, F. Seland, H. Karoliussen, *International Journal of Hydrogen Energy* **2012**, *37*, 18537.

- [7] V. Weissbecker, U. Reimer, K. Wippermann, W. Lehnert, *ECS Transactions* **2013**, *58*, 693.
- [8] D. D. Papadias, R. K. Ahluwalia, J. K. Thomson, H. M. Meyer, M. P. Brady, H. Wang, J. A. Turner, R. Mukundan, R. Borup, *Journal of Power Sources* **2015**, *273*, 1237.
- [9] J. Richards, C. Cremers, P. Fischer, K. Schmidt, *Energy Procedia* **2012**, *20*, 324.
- [10] A. Orsi, O. E. Kongstein, P. J. Hamilton, A. Oedegaard, I. H. Svenum, K. Cooke, *Journal of Power Sources* **2015**, *285*, 530.
- [11] C. Shanmugham, N. Rajendran, *Progress in Organic Coatings* **2015**, *89*, 42.
- [12] M.-T. Lin, C.-H. Wan, W. Wu, *Thin Solid Films* **2013**, *544*, 162.
- [13] B. Caglar, P. Fischer, P. Kauranen, M. Karttunen, P. Elsner, *Journal of Power Sources* **2014**, *256*, 88.
- [14] A. Heinzl, F. Mahlendorf, O. Niemzig, C. Kreuz, *Journal of Power Sources* **2004**, *131*, 35.
- [15] M. Phuangngamphan, M. Okhawilai, S. Hiziroglu, S. Rimdusit, *Journal of Applied Polymer Science* **2019**, *136*, 47183.
- [16] A. Naji, B. Krause, P. Pötschke, A. Ameli, *Polymer Composites* **2018**, *161*, 454.
- [17] A. Bairan, M. Z. Selamat, S. N. Sahadan, S. Malingam, N. Mohamad, *Jurnal Teknologi (Sciences & Engineering)* **2018**, *80*, 115.
- [18] M. N. Akhtar, A. B. Sulong, A. Umer, A. B. Yousaf, M. A. Khan, *Ceramics International* **2018**, *44*, 14457.
- [19] P. Greenwood, R. H. Thring, R. Chen, *Proceedings of the Institution of Mechanical Engineers, Part L: Journal of Materials: Design and Applications* **2012**, *227*, 226.
- [20] A. Hakenjos, H. Muentert, U. Wittstadt, C. Hebling, *Journal of Power Sources* **2004**, *131*, 213.
- [21] C. Hartnig, I. Manke, N. Kardjilov, A. Hilger, M. Grünerbel, J. Kaczerowski, J. Banhart, W. Lehnert, *Journal of Power Sources* **2008**, *176*, 452.
- [22] A. Schröder, K. Wippermann, J. Mergel, W. Lehnert, D. Stolten, T. Sanders, T. Baumhöfer, D. U. Sauer, I. Manke, N. Kardjilov, A. Hilger, J. Schloesser, J. Banhart, C. Hartnig, *Electrochemistry Communications* **2009**, *11*, 1606.
- [23] C. Siegel, G. Bandlamudi, F. Filusch, A. Heinzl, *Fuel Cells* **2011**, *11*, 489.
- [24] L. C. Pérez, J. Ithonen, J. M. Sousa, A. Mendes, *Fuel Cells* **2013**, *13*, 203.
- [25] I. Alaefour, G. Karimi, K. Jiao, S. A. Shakhshir, X. Li, *Electrochimica Acta* **2011**, *56*, 2591.
- [26] A. Phillips, M. Ulsh, J. Porter, G. Bender, *Fuel Cells* **2017**, *17*, 288.
- [27] J. Kleemann, F. Finsterwalder, W. Tillmetz, *Journal of Power Sources* **2009**, *190*, 92.
- [28] I. Nitta, T. Hottinen, O. Himanen, M. Mikkola, *Journal of Power Sources* **2007**, *171*, 26.
- [29] C. Li, E. T. Thostenson, T.-W. Chou, *Applied Physics Letters* **2007**, *91*, 223114.
- [30] Y. Nishi, S. Iizuka, M. C. Faudree, R. Oyama, *Materials Transactions* **2012**, *53*, 940.
- [31] D. Qiu, L. Peng, P. Yi, X. Lai, W. Lehnert, *Energy Conversion and Management* **2018**, *174*, 814.
- [32] M. Z. Chowdhury, O. Genc, S. Toros, *International Journal of Hydrogen Energy* **2018**, *43*, 10798.